ISSN 1070-3284, Russian Journal of Coordination Chemistry, 2017, Vol. 43, No. 11, pp. 770–779. © Pleiades Publishing, Ltd., 2017.

Coordination Polymers of Rare-Earth Elements with 2-Aminoterephthalic Acid[1]

S. Petrosyants*, Zh. Dobrokhotova†, A. Ilyukhin, A. Gavrikov, N. Efimov, and V. Novotortsev

Kurnakov Institute of General and Inorganic Chemistry, Russian Academy of Sciences, Moscow, Russia

**e-mail: petros@igic.ras.ru*

Received May 24, 2017

Abstract—Coordination polymers of REEs with 2-aminoterephthalic acid $[Ln_2(C_8H_5NO_4)_3(H_2O)_5]_n \cdot 2nH_2O$ (Ln = Eu, Gd, or Tb) and $[Y_2(C_8H_5NO_4)_3(H_2O)_4]_n \cdot 4nH_2O$ were prepared by hydrothermal synthesis. Studies of the thermal behavior of these coordination polymers have shown that the removal of the solvate and the coordinated water molecules occurs at heating to 250°C and dehydratation products are stable up to 400°C. Detailed studies of the magnetic behavior of Eu, Gd, and Tb polymers were performed.

Keywords: REE coordination polymers, powder X-ray diffraction studies, thermal decomposition, magnetec studies

DOI: 10.1134/S1070328417110069

INTRODUCTION

At the present time, lanthanide- and yttrium-based carboxylate coordination polymers are among the most interesting and intensively studied coordination compounds. These compounds are of great structural diversity since numerous examples of 1D [1], 2D [2] and 3D polymeric [3] Ln carboxylates are known. They are able to exibit interesting and practically important properties: magnetic [4], luminescent [5], sorptive [6], catalytic [7], etc. Therefore, their potential application as a basis of functional materials is under discussion. Thus, a significant increase in number of studies on the synthesis and study of new polymeric Ln and Y carboxylates with anions of various carboxylic acids (aliphatic acids, aromatic acids, etc.) in recent years is observed.

Among numerous carboxylate ligands, aromatic di- and polycarboxylic acids are widely used to fabricate the coordination polymers [2–4, 7] because of their rich coordination chemistry (variety of their coordination modes), structural rigidity (due to a strong conjugated system), and high affinity between a carboxylate group and a lanthanide ion.

In turn, benzene-1,4-dicarboxylic acid (known as a terephthalic acid) takes a special place among benzenedicarboxylic acids. Its molecular geometry (the O···O spacing exceeding 7 Å) allows formation of polymeric structures with voids up to 10^3 Å. In 2-aminoterephthalic acid (H_2L, $C_8H_7NO_4$), the amino group exhibits a weak coordination ability, but its "active" H atoms are able to form hydrogen bonds (HB) which can affect the channel configuration of a coordination polymers and "capture" solvate molecules containing HB-acceptors in its voids. In all the known coordination polymers of La, Pr, Nd, Eu, Tb, Dy, and Er with H_2L [8–12] synthesized in the absence of competing ligands (except for solvate molecules), the coordination node of Ln is MO_8. The amino-group is not involved in coordination, but it forms the HBs with crystallization water molecules located in 1D channels of the polymers. One N atom of three crystallographically independent L ligands coordinates Ln only in three isostructural $[Ln_2(L)_3(H_2O)_2]_n \cdot 0.5n(4,4'\text{-Bipy}) \cdot n(H_2O)$ compounds (Ln = Eu, Gd, Yb) [13] of 39 Ln complexes with L (including those with competing ligands) (CSD, version 5.36, November 2014 [14]).

In present work, we expanded the series of the REE aminoterephthalate complexes using a modified synthesis procedure which allowed us to obtain the single-phase products in almost quantitative yields. Besides, magnetic properties of Eu, Gd, and Tb-containing compounds with H_2L were studied and discussed for the first time.

EXPERIMENTAL

Materials and physical methods. Commercially available M_2O_3 (M = Y, Eu, Gd, Tb) (Merck) and H_2L (Aldrich) were used for synthesis. Elemental analysis was carried out on an EA1108 85 automatic C, H, N, S analyzer (Carlo Erba Instruments). Attenuated total

[1] The article is published in the original.

† Deceased.

reflection infrared (ATR-IR) spectra were recorded in the range of 400–4000 cm^{-1} on a Bruker ALPHA instrument. The thermal decomposition of compounds was studied by means of differential scanning calorimetry (DSC) and thermogravimetry analysis (TGA) under a flow (20 mL/min) of artificial argon. TGA measurements were performed on TG 209 F1 instrument in alundum crucibles at a heating rate of 10°C/min. The composition of the gas phase was studied on a QMS 403C Aëolos mass spectrometer under TGA conditions. The ionizing electron energy was 70 eV; the largest determined mass number (the mass-to-charge ratio) was 300 a.m.u. DSC study was carried out on DSC 204 F1 instrument in aluminum cells at a heating rate of 10°C/min. Each experiment was repeated at least three times. Data of thermal analysis were analyzed according to the ISO 11357-1, ISO 11357-2, ISO 11358, and ASTM E 1269-95 standards using the NETZSCH Proteus Thermal Analysis software package. Magnetic susceptibility measurements were performed on a Quantum Design MPMS-XL SQUID magnetometer and a Quantum Design PPMS-9 susceptometer. These instruments operate between 1.8 and 400 K for dc applied fields ranging from –7 to 7 T (MPMS-XL) and –9 to 9 T (PPMS-9). For ac susceptibility measurements, an oscillating ac field of 1 or 6 Oe with a frequency between 10 and 10000 Hz (PPMS) were employed. The measurements were performed on polycrystalline samples sealed in a polyethylene bag and covered with mineral oil in order to prevent a field-induced torque of the crystals. Prior to the experiments, the field-dependent magnetization was measured at 100 K in order to detect ferromagnetic impurities. The samples appeared to be free of significant ferromagnetic impurities. The magnetic data were corrected for the sample holder, the mineral oil, and the diamagnetic contribution.

Synthesis of compounds $[Ln_2(C_8H_5NO_4)_3(H_2O)_5]_n \cdot 2nH_2O$ (Ln = Eu (I), Gd (II), or Tb (III)). To the Ln_2O_3 (0.181 g (0.515 mmol) Eu_2O_3; 0.180 g (0.498 mmol) Gd_2O_3; 0.188 g (0.51 mmol) Tb_2O_3), stoichiometric ammount of H_2L (1.5 mmol) and H_2O (15–20 mL) were added. The resulting slurry was stirred for 30 min, then placed in a Teflon autoclave and allowed to stand at 170°C for 72 h. The resulting solid phase was washed with H_2O and EtOH, and dried in air. The yields of **I** (sand-yellow), **II** (sand-colored), and **III** (sand-colored) were 0.43 g (86.3% based on Eu), 0.39 g (80.0% based on Gd), and 0.45 g (88.0% based on Tb), respectively.

Compound $[Y_2(C_8H_5NO_4)_3(H_2O)_4]_n \cdot 4nH_2O$ (**IV**) was synthesized similarly to **I**–**III** using 0.280 g (1.55 mmol) of H_2L and 0.120 g (0.53 mmol) of Y_2O_3. The yield of **IV** (cacao-colored) was 0.35 g (82.0% based on Y).

For $C_{24}H_{29}N_3O_{19}Eu_2$ (**I**; $M = 967.42$)

Anal. calcd., %:	C, 29.79;	H, 3.02;	N, 4.34.
Found, %:	C, 30.66;	H, 4.00;	N, 4.25.

IR of **I** (ν, cm^{-1}): 3320 br. w, 1621 w, 1521 s, 1493 s, 1425 s, 1371 vs, 1327 s, 1256 s, 1153 w, 1045 w, 962 w, 891 w, 834 m, 817 w, 803 m, 769 s, 700 m, 670 m, 576 s, 554 s, 503 vs, 433 s, 409 s.

For $C_{24}H_{29}N_3O_{19}Gd_2$ (**II**; $M = 977.99$)

Anal. calcd., %:	C, 29.47;	H, 2.99;	N, 4.29.
Found, %:	C, 30.66;	H, 4.00;	N, 4.25.

IR of **II** (ν, cm^{-1}): 3316 br. w, 1621 w, 1518 s, 1493 s, 1422 s, 1371 s, 1325 s, 1252 s, 1151 m, 1123 m, 1048 m, 960 m, 889 w, 834 m, 817 m, 804 m, 793 m, 765 s, 714 m, 698 m, 673 m, 572 s, 555 s, 500 vs, 433 s, 406 s.

For $C_{24}H_{29}N_3O_{19}Tb_2$ (**III**; $M = 981.35$)

Anal. calcd.,%:	C, 29.37;	H, 2.98;	N, 4.28.
Found, %:	C, 29.28;	H, 4.36;	N, 4.41.

IR of **III** (ν, cm^{-1}): 3324 br. w, 1619 m, 1535 s, 1495 s, 1423 s, 1378 vs, 1331 s, 1284 m, 1249 s, 1153 w, 1048 w, 963 w, 933 w, 892 w, 850 m, 834 m, 818 w, 806 m, 769 s, 687 m, 675 m, 633 m, 613 s, 578 s, 565 s, 503 vs, 432 s, 409 s.

For $C_{24}H_{31}N_3O_{20}Y_2$ (**IV**; $M = 859.32$)

Anal. calcd., %:	C, 33.54;	H, 3.63;	N, 4.88.
Found, %:	C, 32.34;	H, 4.25;	N, 4.76.

IR of **IV** (ν, cm^{-1}): 3323 br. w, 1620 m, 1541 s, 1497 s, 1423 s, 1381 vs, 1335 m, 1249 m, 1154 w, 964 w, 894 w, 852 m, 837 m, 804 m, 769 s, 695 m, 671 m, 627 m, 610 s, 583 s, 564 s, 507 vs, 434 s, 405 vs.

Powder X-ray diffraction. The powder X-ray diffraction studies were performed on a Bruker D8 ADVANCE X-ray diffractometer (CuK_α, Ni-filter, LYNXEYE detector, reflection geometry) at UFC IGIC RAS. The unit cell parameters for compounds **I**–**IV** were obtained by the full-profile refinement using the Rietveld method (Fig. 1). The atomic coordinates were taken from structures of $[Pr_2L_3(H_2O)_5]_n \cdot 2nH_2O$ [8] and $[Dy_2L_3(H_2O)_4]_n \cdot 4nH_2O$ [12] and fixed. All calculations were carried out using the TOPAS software [15] (Table 1).

RESULTS AND DISCUSSION

For syntheses of the benzenedicarboxylate coordination polymers, corresponding acids (which are water-insoluble) are usually preliminarily converted

into soluble salts, or syntheses are conducted in the presence of bases, i.e., hydrothermal syntheses proceed in MX_3 (X = Cl, NO_3)–ligand–base (NaOH, KOH) solutions. In accordance to the latter procedure, the complex of Tb with H_2L was synthesized [8]. But the yield of the coordination polymers obtained according to such procedure is given only in [10]: 54% for the erbium coordination polymers with H_2L. We simplified the synthesis by replacing MX_3 with M_2O_3, thus excluding the stage of ligand deprotonation. The modified procedure allowed us to obtain single-phase products with much higher yields (up to 90%). Its worth mentioning that all the syntheses were performed at the H_2L : M_2O_3 ratio of ~3 and heterogeneous slurries had pH 5 before and after the syntheses.

Compounds **I–IV** have similar IR spectra. Broad blurred absorption bands in the 3400–3210 cm^{-1} range are assigned to the stretching vibrations of coordination and outer-sphere water molecules; individual narrow bands due to the deformation vibrations of water molecules $\delta(H_2O)$ are observed at 1621, 1621, 1619, and 1620 cm^{-1} for **I–IV**, respectively. The complex $\{\nu(C{=}O)_{COOH} + \delta(NH_3^+)\}$ band at 1668 cm^{-1} in the spectrum of the aminoterephthalic acid disappears in the spectra of **I–IV** indicating that the ligand is completely deprotonated in all the four complexes. In addition, the intense bands assigned to the asymmetric (ν_{as}, 1490–1520 cm^{-1}) and the symmetric (ν_s, 1370–430 cm^{-1}) stretching vibrations of deprotonated carboxylic groups COO^- are observed in the spectra of **I–IV**. The bands in the range 800–460 cm^{-1} assigned to the deformation vibrations of carboxylic groups, $\delta(COO)$, are symbatically shifted to larger wavelengths (503, 700, and 769 cm^{-1} for **I**) compared to the corresponding bands in the spectrum of free H_2L (489, 677, and 751 cm^{-1}).

At the present time, three structural types of coordination polymers obtained in the Ln–H_2L–H_2O system are known: $[Ln_2L_3(H_2O)_4]_n \cdot 4nH_2O$ (Ln = Nd [11]; Eu, Tb [8], Dy [12]) and $[Er_2L_3(H_2O)_4]_n \cdot 1.5nH_2O$ [10] (type **A**); $[Ln_2L_3(H_2O)_5]_n \cdot 2nH_2O$ (Ln = La [9], Pr [8]) (type **B**); and $[Pr_3(HL)_4(L)_2]_n(NO_3)_n \cdot 8nH_2O$ [16], $[Nd(HL)(L)]_n \cdot 3nH_2O$ [16], and $[Ln(HL)(L)]_n \cdot xnH_2O$ (Ln = La–Sm excluding Pm) [17] (type **C**). Hydrothermal synthesis results in structures **A** and **B**. Compounds of type **C** were obtained under normal pressure.

In all three structural types, molecular complexes are connected into 3D frameworks involving solvate water molecules. In all compounds, the L ligands are disordered so that each amino-group occupies two or three positions. Molecules of crystallization water are disordered. The composition of $[Pr_3(HL)_4(L)_2]_n(NO_3)_n \cdot 8nH_2O$ [16] seems doubtful, since the disordering of the structure does not allow one to unambiguously localize the nitrate ion.

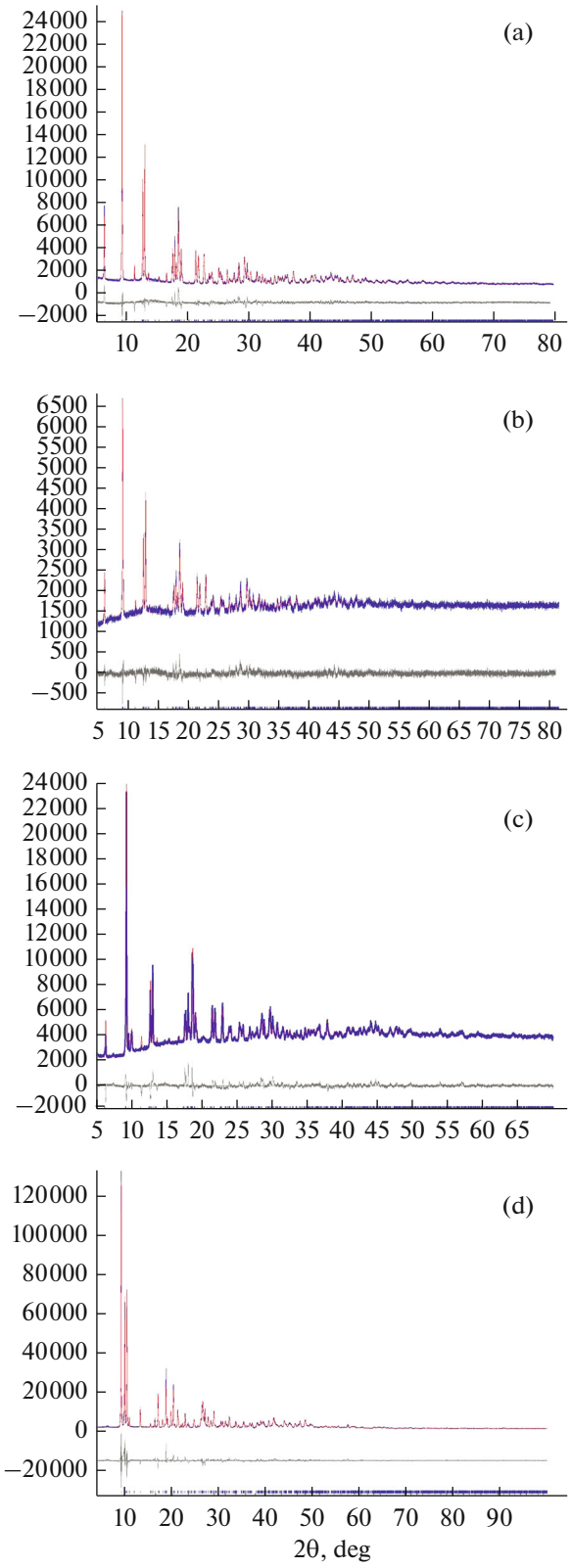

Fig. 1. Rietveld refinement profiles for **I** (a), **II** (b), **III** (c), and **IV** (d) for room temperature X-ray data, respectively. The bottom trace shows the difference curve. The vertical bars indicate the calculated positions of the Bragg peaks.

Table 1. Crystallographic data and structure refinement for **I**–**IV**

Parameter	Value			
	I	**II**	**III**	**IV**
Empirical formula	$C_{24}H_{29}N_3O_{19}Eu_2$	$C_{24}H_{29}N_3O_{19}Gd_2$	$C_{24}H_{29}N_3O_{19}Tb_2$	$C_{24}H_{31}N_3O_{20}Y_2$
Formula weight	967.42	978.00	981.35	859.32
Temperature, K	296	296	296	296
Wavelength, Å	1.5419	1.5419	1.5419	1.5419
Crystal system	Triclinic	Triclinic	Triclinic	Triclinic
Space group	$P\bar{1}1$	$P\bar{1}$	$P\bar{1}$	$P\bar{1}$
a, Å	10.31154(18)	10.2907(4)	10.2665(4)	10.1150(2)
b, Å	15.1381(2)	15.1330(5)	15.1373(6)	10.31841(16)
c, Å	10.0722(2)	10.0598(4)	10.0354(4)	9.4398(2)
α, deg	101.687(2)	101.843(5)	101.976(6)	95.413(2)
β, deg	100.458(2)	100.254(5)	100.024(5)	110.2800(19)
γ, deg	106.1829(17)	106.234(3)	106.346(4)	110.7603(17)
Volume, Å^3	1430.51(6)	1425.18(11)	1418.38(12)	837.25(4)
Z	2	2	2	2
θ Range, deg	5–80	5–80	5–70	4–100
Step size 2θ, deg	0.005	0.005	0.008	0.005
Parameters	20	21	35	28
R-Bragg	3.385	1.646	3.175	4.628
R_{exp}	2.75	2.45	1.58	1.77
R_{wp}	6.49	3.26	3.88	8.90
R_p	4.65	2.51	2.56	6.29
GOOF	2.36	1.33	2.46	5.03

In the structural type **A**, there are three crystallographically independent L ligands per one Ln atom. These ligands are located in the inversion centers, and their NH_2 groups are therefore disordered. In addition to the six carboxylate O atoms of three L ligands, the Ln coordination environment also includes two H_2O molecules. The coordination number of Ln is 8 + 1 (Fig. 2). The Ln(1)–O(5) distance is 3.03 Å (Ln = Nd [11]).

Stuctures of **B** type are formed by two crystallographically independent eight-coordinate Ln atoms and three independent L ligands (Fig. 3a; Ln = Pr [8]). Although the three ligands are located at general positions, all of them are disordered: NH_2 group is statistically bound to carbon atoms in positions 2 and 5, i.e., the local symmetry of the ligand is $\bar{1}$. Eleven of twelve carboxylate O atoms of L ligands are coordinated by Ln; O(4) is the only oxygen atom uninvolved in coordination. Ln(1) and Ln(2) atoms additionally coordinate two and three H_2O molecules, respectively.

It was suggested [8] that the **B**→**A** morphotropic transition takes place between Pr and Nd; however, our data revealed the existence of both phases for Eu–Tb. Thus, structures of **A** type are known for Y and Nd–Er and structures of **B** type are known for La–Tb.

Single-phase complexes **I** and **II**, as well as almost single-phase complex **III** (>95%), obtained in this study belong to type **B**. Initially, the synthesis of the Gd complex afforded a mixture of the **A** and **B** modifications; i.e., both modifications are formed simultaneously and under the same conditions. By varying synthetic conditions, we isolated single-phase specimen of **II**. Attempts to obtain pure **A** form failed, therefore, it can be assumed that form **B** is more stable. Structural comparison of the phases provides an indirect support for this assumption. The coordination number of Ln atoms is 8 + 1 in complexes of **A** form and 8 in complexes of **B** form; i.e., in accordance with the lanthanide contraction, forms **A** and **B** are more favorable for light and heavy lanthanides, respectively. However, available experimental data show the opposite picture. Unfortunately, powder XRD patterns are not given in [8, 9, 11, 12]; therefore, we can not estimate the purity of the compounds reported there. The powder pattern of compound $[Er_2L_3(H_2O)_4]_n \cdot 1.5nH_2O$ [10] suggests that a mixture of forms **A** and **B** was isolated: the multiplet consisting of four peaks in

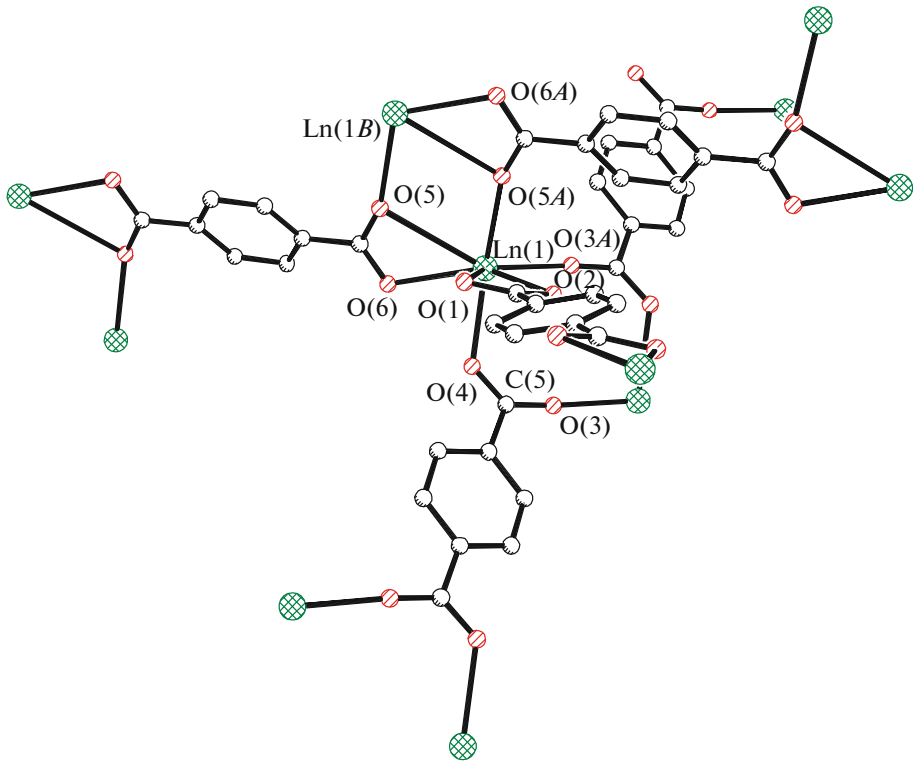

Fig. 2. Fragment of structural type **A** (coordinated H_2O molecules, H atoms and NH_2 groups are omitted).

the $2\theta = 9°–11°$ range makes it similar to the powder pattern of the mixture of the two forms of Gd complex obtained in the present study.

In all syntheses, complex **III** (Fig. 1) is accompanied by an unknown crystal phase. Magnetic susceptibility (see below) was measured for a sample with its minimal content (~4%) on the assumption that the impurity has the same scattering power as complex **III**. Note that the similar impurity was formed in some syntheses of the Eu complex. Because of the large volume of the triclinic unit cell of the **B** type structures (1450 Å^3), many peaks on the X-ray pattern overlap; we distinguished only six peaks that are unambiguously attributed to the unknown phase. The doublet at D ~ 9 Å indicates that the asymmetric unit of the unknown impurity has a large volume, and, as a consequence, six lines are insufficient to perform cell indexing.

According to the Rietveld refinement (Fig. 1), the sample of complex $[Y_2L_3(H_2O)_4]_n \cdot 4nH_2O$ contained 8.5(1)% of Y_2O_3.

Studies of the thermal behavior of coordination polymers **I–IV** revealed that their thermal stability is determined by the presence of solvate water molecules. For all the compounds under study, regardless of the structural type, the removal of solvate molecules (according to the data of TGA) begins at 50 ± 3°C (Fig. 4). The removal of coordinated water molecules takes place above 140 ± 3°C. The mass spectrum of the gaseous phase under the conditions of thermogravimetric experiment in the temperature range of 50–250°C corresponds to the mass spectrum of water. The resulting dehydration products remain stable up to 400°C when destructive removal of the organic fragments starts.

In order to characterize possible structures of intermediates, a comparative study of IR spectra (ATR-IR) of starting $[Ln_2(C_8H_5NO_4)_3(H_2O)_5]_n \cdot 2nH_2O$ complexes and products of their complete dehydration $\{Ln_2(C_8H_5NO_4)_3\}$ was performed. Fragments of the IR spectra of complex **II** and corresponding intermediate are shown in Fig. 5. It can be seen that the broad band in the 3300–3400 cm^{-1} region in IR spectra of complex **II** (assigned to the stretching vibrations of water molecules) disappears after dehydration and two previously masked sharp separate bands (3484 and 3369 cm^{-1}) assigned to the ν(N–H) stretching vibrations of free amino groups of aminoterephthalate ions appear. The band at 1621 cm^{-1} assigned to the deformation vibrations of water molecules, δ(H_2O), also disappears in the spectrum of the intermediate.

At the same time, it can be assumed that the coordination of carboxylic groups remains almost unchanged, as it can be concluded from rather close coincidence of the position and shape of the bands corresponding to their stretching vibrations.

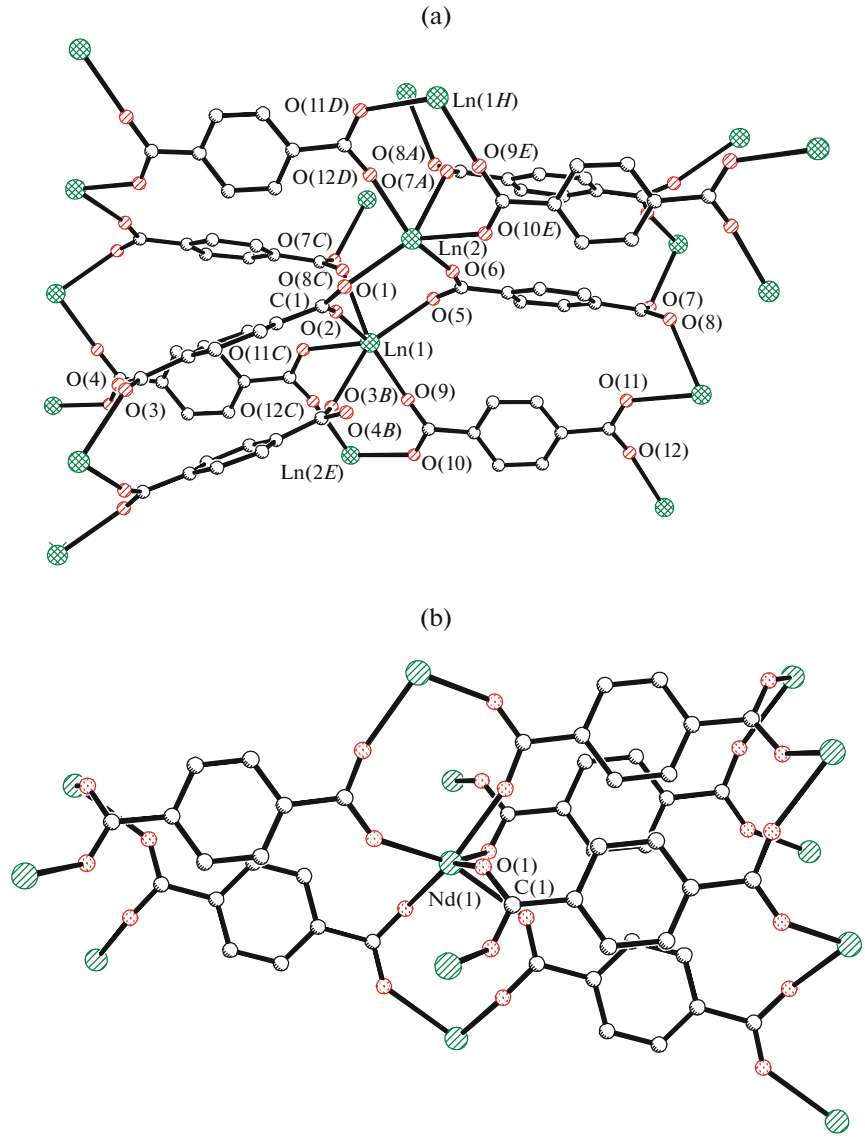

Fig. 3. Fragments of (a) structural type **B** and (b) structure $[Nd_2(TPh)_3(H_2O)_4]$ [18] (coordinated H_2O molecules, H atoms and NH_2 groups are omitted).

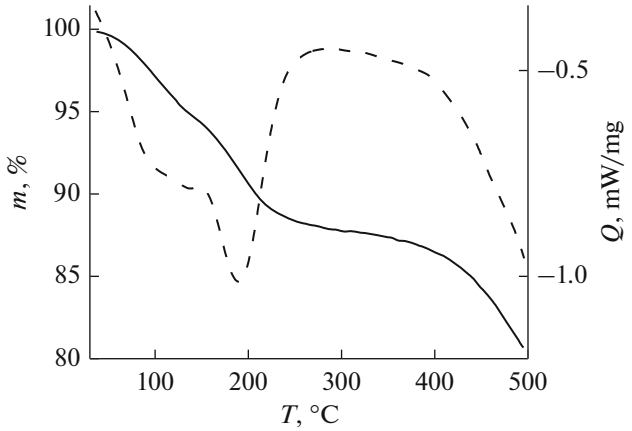

Fig. 4. DSC (dashed) and TGA (solid) curves for complex **II** in the temperature range 20–500°C.

Actually, if all water molecules are removed from the **B** type structure, the coordination numbers of Ln(1) and Ln(2) atoms lower to six and five, respectively. However, the process of dehydration is accompanied by the adjustment movement of structural units. Thus, it can be assumed that upon dehydration the noncoordinated O(4) atom enters the Ln(2) coordination sphere, thereby increasing the coordination number to six (Fig. 3a). In this hypothetical structure, all 12 oxygen atoms of three L ligands are coordinated by Ln atoms. Such ligand coordination was found in compound $[Nd_2(TPh)_3(H_2O)_4]$ [18], where TPh^- is the terephthalate anion. The TPh^- ligand can be considered as a crystal-chemical analog of the aminoterephthalate ligand L, since the disordered amino-group of the L ligand is uninvolved in metal coordination

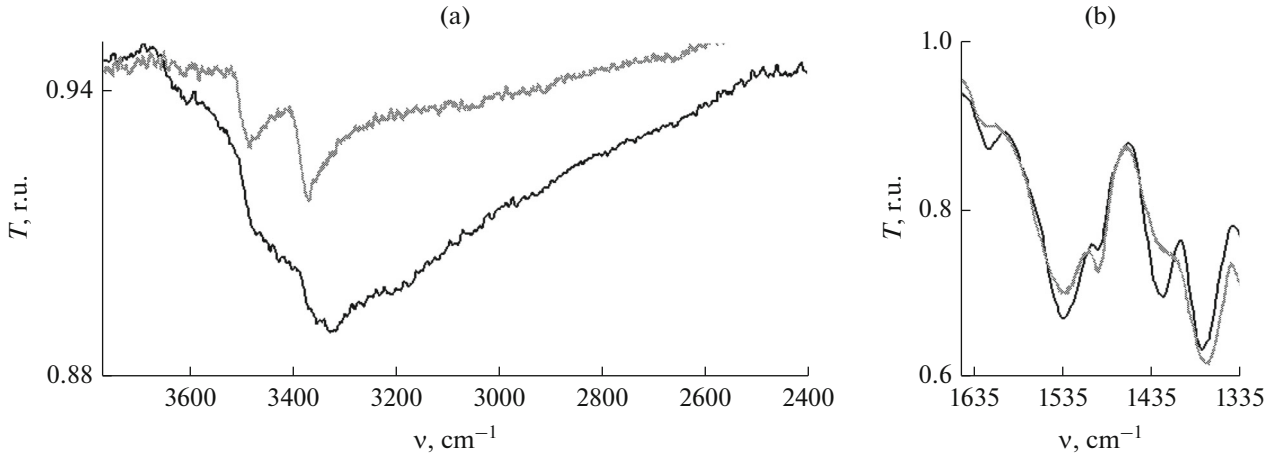

Fig. 5. Fragments of IR spectra of $[Gd_2(C_8H_5NO_4)_3(H_2O)_5]_n \cdot 2nH_2O$ (*1*) and $\{Gd_2(C_8H_5NO_4)_3\}$ (*2*) in the range of 3770–2400 cm^{-1} (a) and 1650–1335 cm^{-1} (b).

both in complexes of the **A** and **B** types. In compound $[Nd_2(TPh)_3(H_2O)_4]$ [18], the coordination number of Nd is 8: the coordination environment is formed by six O atoms of the carboxylic groups of TPh^- and two O atoms of H_2O molecules (Fig. 3b). Coordination number of 6 is not typical of Ln complexes synthesized in donor solvents media, but it is known for compounds obtained by sublimation, for example, $[Yb(Acac)_3]$ [19]. On the other hand, a slight shift of Ln "layers" relative to one another (the "layers" are perpendicular to the plane of the drawing in Fig. 3a) can change the function of carboxylic groups from bridging to chelate-bridging (like that of the O(5,6) group in Fig. 1) and thereby increase the coordination number of Ln to 7 or 8.

The magnetism of Ln(III) complexes results from the electronic structure of free lanthanide ions itself and mostly is determined by the spin-orbit interactions. The spin-orbit coupling constants of lanthanides are equal to thousands of inverse centimeters. Hence, the energy splitting between multiplets is large as compared to kT, and only the ground state is populated at room and lower temperatures for most of free lanthanide ions. As a result, in the majority of cases, the experimental values of the effective magnetic moments of trivalent lanthanide compounds are described by the equathion $\mu = g[J(J+1)]^{1/2}$, where J is the total momentum of the ground state and g is the g factor of this state [20].

In contrast with other Ln^{3+} ions, compounds with Eu^{3+} ($4f^6$) are characterized by a small splitting between the non-magnetic ground-state $^7F_0$ and the first excited multiplets (400 cm^{-1}) [21]. The magnetic behavior of complex $[Eu_2(C_8H_5NO_4)_3(H_2O)_5]_n \cdot 2nH_2O$ (**I**) is typical for Eu(III) compounds. The $\chi_m T(T)$ and $\chi_m(T)$ plots for europium complex **I** are shown in Fig. 6. Considering the following spin-orbit Hamiltonian $H_{SO} = \lambda \mathbf{LS}$, the first excited $^7F_1$ state is only λ cm^{-1} higher in energy than the $^7F_0$ level. Up to 300 K, the thermal energy suffices to populate significantly only three first energy levels (0, λ, and 3λ) inducing a significant magnetic moment at room temperature as observed in Fig. 5 for **I** [22]. As expected in the case for which kT is of the order of λ, the room temperature value of the $\chi_m T$ product (1.36 cm^3 K mol^{-1}) does not reach the theoretical high temperature limit, $12N_A\mu_B^2/k_B$, i.e., 4.5 cm^3 K mol^{-1} [22]. A monotonic decrease of the χT product is observed with lowering of the temperature between 300 and 2 K, at which it reaches 0.0014 cm^3 K mol^{-1}. As observed for similar Eu(III) complexes, this decrease corresponds to the depopulation of the magnetic low lying excited levels. Based on the energy spectra obtained from the spin-orbit Hamiltonian, H_{SO}, the theoretical temperature dependence of the magnetic susceptibility can be calculated in the weak-field approximation using the van Vleck equation [22]. Only one parameter, the spin-orbit coupling constant λ, is necessary to simulate the experimental data, which are fitted perfectly with $\lambda = 344 \pm 1$ cm^{-1} (see line in Fig. 6). The energy difference between the $^7F_0$ and $^7F_1$ levels estimated from the magnetic susceptibility at low temperatures (between 70–30 K, $\chi \approx 6.2 \times 10^{-3}$ cm^3 mol^{-1}) using the known Caro-Porcher equation is 339 cm^{-1}. This value is in a good agreement with the λ value found from the $\chi_m T(T)$ and with literature estimations [22].

Compounds containing Gd^{3+} ion are distinguished among complexes with $4f$ ions due to specific features of the electronic structure of this ion. The Gd^{3+} ion has the maximum possible number of unpaired electrons ($S = 7/2$) in a series of f elements and this ion is isotropic. Therefore, the contribution of the spin-orbit interaction is absent for Gd^{3+}. For complex

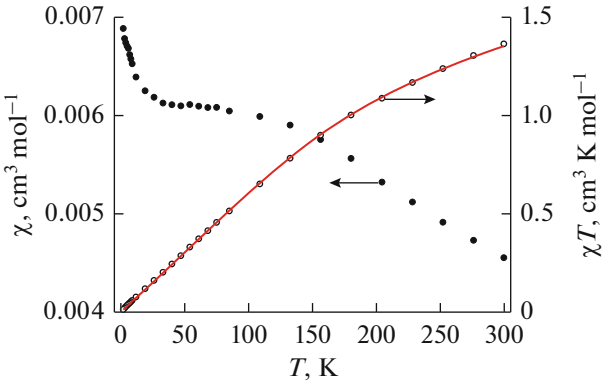

Fig. 6. Temperature dependences of the χ (●) and the χ*T* (○) product (where χ is the molar magnetic susceptibility equal to *M*/*H* per Eu^{3+} ion) measured at 0.5 *T* for **I**. The solid line is the best fit of the experimental data for **I** to the model described in the text.

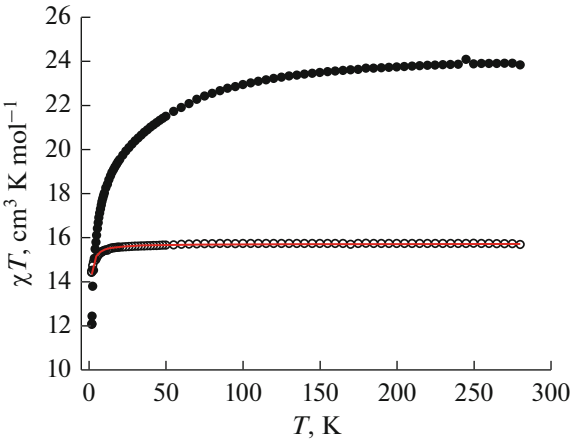

Fig. 7. Temperature dependences of the $\chi_m T$ for $[Gd_2(C_8H_5NO_4)_3(H_2O)_5]_n \cdot 2nH_2O$ (**II**) (○) and $[Tb_2(C_8H_5NO_4)_3(H_2O)_5]_n \cdot 2nH_2O$ (**III**) (●) measured at $H = 0.1$ T. The solid line is the best fit of the experimental data for **II** to the model described in the text.

$[Gd_2(C_8H_5NO_4)_3(H_2O)_5]_n \cdot 2nH_2O$ (**II**), the temperature dependence of the dc magnetic susceptibility was studied in the temperature range 300–2 K under an applied magnetic field of 1 kOe (Fig. 7).

The value of $\chi_m T$ for complex **II** at room temperature is 15.69 cm^3 K mol^{-1} which is close to the calculated value for Gd^{3+} ion (15.76 cm^3 mol^{-1} K ($S = 7/2$, L = 0, $^8S_{7/2}$, $g = 2$, $C = 7.9$ cm^3 K mol^{-1})). It remains virtually constant as the temperature lowers to 20 K ($\chi_m T$ (20 K) = 15.60 cm^3 K mol^{-1}) and then abruptly decreases reaching 14.45 cm^3 K mol^{-1} at 2 K. The temperature-independent behavior (300–20 K) suggests that the coupling between the Gd^{3+} ions is very weak as it has been observed for many polynuclear Gd(III) complexes [23]. The exchange interactions were evaluated using the model of chains of equally spaced magnetic centers with local spins larger than 1/2. As the complex consists of infinite chains with equal spacings, it can be quantitatively analysed using equation (1) [22]:

$$\chi T(T) = \frac{Ng^2\beta^2 S(S+1)}{3k} \times \frac{1+\coth\left[\frac{JS(S+1)}{kT}\right] - \frac{kT}{JS(S+1)}}{1-\coth\left[\frac{JS(S+1)}{kT}\right] + \frac{kT}{JS(S+1)}}, \quad (1)$$

where *N* is the Avogadro constant; *g* is the *g* factor; β is the Bohr magneton; *k* is the Boltzmann constant; and *J* is the isotropic interaction parameter. The best agreement between the experimental and theoretical data was obtained with the $g = 2.00 \pm 0.01$ and $J = -0.012 \pm 0.001$ cm^{-1} (Fig. 7).

The field dependence of the magnetization *M*(*H*) for **II** was studied at *T* = 1.85, 3, 5, and 8 K in the magnetic fields up to $H_{max} = 70$ kOe (see inset in Fig. 8).

According to [22], the field dependences of magnetization are described by the Brillouin function if there are no significant magnetic interactions in a system. The field dependences of the magnetization represented in the form of the $M = f(H/T)$ curves should coincide at any temperature. Close coincidence of all $M = f(H/T)$ curves (Fig. 8) confirms that there are no significant interactions in the $[Gd_2(C_8H_5NO_4)_3(H_2O)_5]_n \cdot 2nH_2O$ complex. The Brillouin function (Fig. 8) was plotted for $g = 2$ and $J = 7/2$ at $T = 1.85$ K. Slight deviation of the Brillouin function from the experimental curve to lower values at magnetic fields $H > 1$ *T* can be explained by the fact that the *g* factor of the complex studied slightly exceeds $g = 2$.

For complex $[Tb_2(C_8H_5NO_4)_3(H_2O)_5]_n \cdot 2nH_2O$ (**III**), the $\chi_m T$ product remains almost constant down to 160 K (25.0 cm^3K/mol), then decreases slowly with temperature lowering, and at ~10 K sharply decreases reaching 13.3 cm^3 K/mol at 2 K (Fig. 7). Such decreasing can be attributed to the zero-field splitting effects (under the effect of the ligands field), Zeeman effects from the applied magnetic field and/or to possible antiferromagnetic coupling between the lanthanide ions [24].

The $M = f(H/T)$ dependences for complex $[Tb_2(C_8H_5NO_4)_3(H_2O)_5]_n \cdot 2nH_2O$ (**III**) are shown in Fig. 9. The difference between the curves obtained at different temperatures is observed. Thus, the noticeable magnetic anisotropy and the existence of a certain energy barrier Δ*E*, which has to be overcome for the reorientation of the magnetic moment of the molecule could be expected for complex **III**. However, the measurements of the dynamic (AC) magnetic susceptibility did not reveal slow magnetic relaxation, and a noticeable deviation of the out-of-phase magnetic

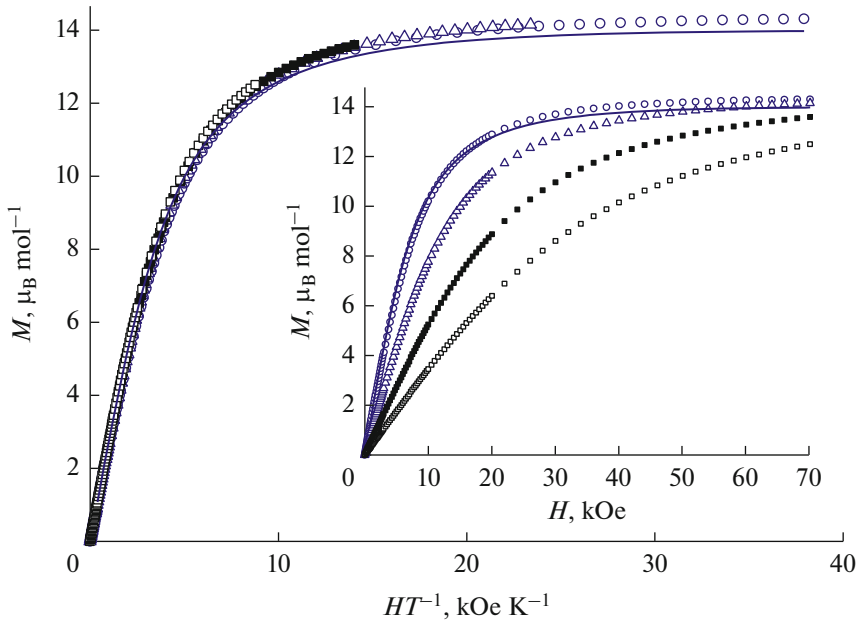

Fig. 8. Field dependences of the magnetization for complex $[Gd_2(C_8H_5NO_4)_3(H_2O)_5]_n \cdot 2nH_2O$ (**II**) plotted as M vs. H/T and M vs. H (inset) at $T = 1.85$ (○), 3 (△), 5 (■), and 8 (□) K. The Brillouin function for $g = 2$ and $J = 7/2$ at $T = 1.85$ K is shown as a solid line.

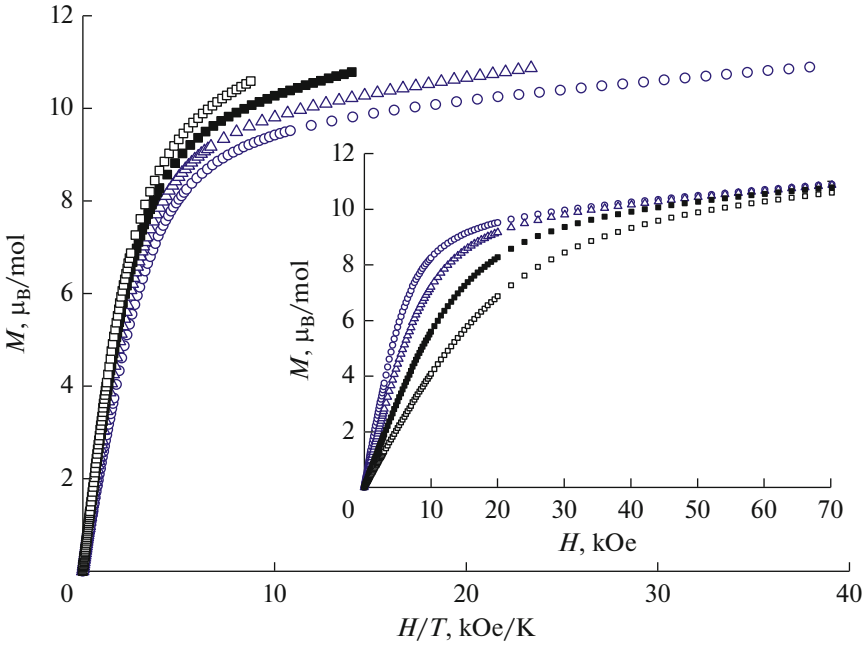

Fig. 9. Field dependences of the magnetization for complex $[Tb_2(C_8H_5NO_4)_3(H_2O)_5]_n \cdot 2nH_2O$ (**III**) plotted as M vs. H/T and M vs. H (inset) at $T = 1.85$ (○), 3 (△), 5(■), and 8 K (□).

susceptibility χ" from zero was found only at $T = 1.9$ K in a magnetic field of 3500 Oe.

Therefore, the results of the present study of the magnetic behavior of the coordination polymers **I**–**III** confirm the regularities of the changes in the magnetic behavior in accordance with the nature of the lanthanide ion itself.

In summary, a new approach to the hydrothermal synthesis of coordination polymers based on REEs and 2-aminoterephthalic acid was proposed. Using of

REE oxides as starting reagents allows one to exclude competing acido ligands and to attain almost quantitative yields of the single-phase products. The REE coordination polymers with 2-aminoterephthalic acid prepared under hydrothermal conditions exhibit polymorphism. The coordination polymer of Gd (**II**) was obtained as a mixture of **A** and **B** modifications, and further optimization of the synthesis conditions allowed us to obtain the single-phase product **B**. The dehydration of coordination polymers **I**–**IV** finishes up to 250°C, and the intermediates remain stable up to 400°C. Detailed studies of magnetic susceptibility (DC) were performed for the complexes containing paramagnetic Eu^{3+} (**I**), Gd^{3+} (**II**), and Tb^{3+} (**III**) ions. The magnetic behavior of complex **I** is typical of Eu(III) compounds. For **I**, the spin-orbit coupling constant λ was calculated using the van Vleck equation in the weak-field approximation and the energy difference between the $^7F_0$ and $^7F_1$ levels λ_{C-P} was estimated using the Caro-Porcher equation. The calculated values of λ and λ_{C-P} are in a good agreement. Studies of complex **II** did not reveal significant exchange interactions. Noticeable magnetic anisotropy and the existence of the certain energy barrier which has to be overcome for the reorientation of the magnetic moment of the molecule could be expected for complex **III**. However, the measurements of the dynamic (AC) magnetic susceptibility did not reveal slow magnetic relaxation, and a noticeable deviation of out-of-phase magnetic susceptibility χ'' from zero was found only at $T = 1.9$ K in an external magnetic field of 3500 Oe.

ACKNOWLEDGMENTS

This study was supported by the Russian Science Foundation (project 14-13-00938). This work was partially performed using the equipments of the Joint Research Centre of IGIC RAS. Authors thank Mathieu Rouzières and Rodolphe Clérac from Centre de Recherche Paul Pascal (Pessac, France) for their help in magnetic measurements.

REFERENCES

1. Rohde, A., Hatscher, S.T., and Urland, W., *J. Alloys Comp.*, 2004, vol. 374, p. 137.
2. Ying-Bing Lu, Lei-Peng Chen, Shi-Yong Zhang, et al., *Z. Anorg. Allg. Chem.*, 2015, vol. 641, p. 2408.
3. Jia-Jun Yang, Xiao-Yang Yu, Yu-Hui Luo, et al., *Inorg. Chem. Commun.*, 2015, vol. 61, p. 16.
4. Ying-Bing Lu, Shuang Jin, Zhong-Gao Zhou, et al., *Inorg. Chem. Commun.*, 2014, vol. 48, p. 73.
5. Freslon, S., Yun, Luo., Daiguebonne, C., et al., *Inorg. Chem.*, 2016, vol. 55, p. 794.
6. Xiaohui, Yi., Bernot, K., and Calvez, G., *Eur. J. Inorg. Chem.*, 2013, p. 5879.
7. Shengyan Wang, Jianing Xu, Jifu Zheng, et al., *Inorg. Chim. Acta*, 2015, vol. 437, p. 81.
8. Xu Haitao, Zheng Nengwu, Jin Xianglin, et al., *J. Mol. Struct.*, 2003, vol. 655, p. 339.
9. Xu Haitao, Zheng Nengwu, Jin Xianglin, et al., *Chem. Lett.*, 2002, p. 350.
10. Yonggang Wu, Nengwu Zheng, Ruyi Yang, et al., *J. Mol. Struct.*, 2002, vol. 610, p. 181.
11. Hai Tao Xu, Neng Wu Zheng, Jin Xiang Lin, et al., *J. Mol. Struct.*, 2003, vol. 654, p. 183.
12. Hai Tao Xu, Neng Wu Zheng, Xiang Lin Jin, et al., *J. Mol. Struct.*, 2003, vol. 646, p. 197.
13. Liu, C.-B., Zheng, X.-J., Yang, Y.-Y., and Jin, L.-P., *Inorg. Chem. Commun.*, 2005, vol. 8, p. 1045.
14. Allen, F.H., *Acta Crystallogr., Sect. B: Struct. Sci.*, 2002, vol. 58, p. 380.
15. *TOPAS*, Bruker AXS, Karlsruhe, 2005.
16. Chen, X.-Y., Zhao, B., Shi, W., et al., *Chem. Mater.*, 2005, vol. 17, p. 2866.
17. Luo, Y., Calvez, G., Freslon, S., et al., *Inorg. Chim. Acta*, 2011, vol. 368, p. 170.
18. Zehnder, R.A., Renn, R.A., Pippin, E., et al., *J. Mol. Struct.*, 2011, vol. 985, p. 109.
19. Batsanov, A.S., Struchkov, Y.T., Trembovetskii, G.V., et al., *Dokl. Akad. Nauk SSSR*, 1986, vol. 289, p. 903.
20. Van Vleck, J.H., *The Theory of Electric and Magnetic Susceptibilities*, Oxford: Univ. Press, 1932.
21. Zvezdin, A.K., Matveev, V.M., Mukhin, A.A., and Popov, A.I., *Rare-Earth Ions in Magnetically Ordered Crystals*, Moscow: Nauka, 1985.
22. Kahn, O., *Molecular Magnetism*, New York: VCH Publishers, Inc, 1993.
23. Das, A., Dey, S., Biswas, E., et al., *Inorg. Chem.*, 2014, vol. 53, p. 3417.
24. Goura, J., Walsh, J.P.S., Tuna, F., and Chandrasekhar, V., *Inorg. Chem.*, 2014, vol. 53, p. 3385.